Study of ^{9}Be(p,pn) and ^{9}Be($p,2p$) reactions at 70 MeV

V. B. Shostak,[1] G. P. Palkin,[1] N. I. Woloshin,[1] V. P. Likhachev,[2] M. N. Martins,[2] and J. D. T. Arruda-Neto[2]
[1]*Institute for Nuclear Research, Kiev, Ukraine*
[2]*Instituto de Física da Universidade de São Paulo, Laboratório do Acelerador Linear, Caixa Postal 66318, 05315-970 São Paulo, SP, Brazil*

(Received 23 February 1999; published 22 December 1999)

Differential cross sections for the reactions ^{9}Be(p,pn)^{8}Be and ^{9}Be($p,2p$)^{8}Li were simultaneously measured at an incident proton energy of 70 MeV. The measured spectra were decomposed into contributions from $1p$ and $1s$ shells. The cross sections were then analyzed in the framework of the DWTA approach. The radius of ^{8}Be was derived.

PACS number(s): 25.40.Ep, 27.20.+n

I. INTRODUCTION

The quasielastic knockout of a nucleon by high energy protons is a powerful tool in the study of single-particle aspects of the nuclear structure. For incident protons with energies below ~400 MeV, the single-particle character of the proton-nucleon interaction starts to be substantially distorted, due to several effects. Among them are the off-shell effects, when the scattering of two particles is distorted by their interaction with particles of the medium. Another important process is related to the interaction of the outgoing nucleon with the residual nucleus in the final state, the final state interaction (FSI). For incident proton energies below ~100 MeV these distortion effects are the dominant interaction processes and they determine the character of the reaction. Accurate knowledge of the off-shell behavior of the two-nucleon amplitude is necessary for an unambiguous solution of the inverse problem, namely, the reconstruction of the nucleon-nucleon potential from data on nucleon-nucleon scattering. The study of FSI is also interesting, because FSI is sensitive to properties of the residual nucleus, and so may bring information about nuclear interactions or properties of exotic nuclei, for which it would be impossible to prepare a target due to technical or fundamental physical reasons, but could be formed as the residual nucleus in a knockout process.

The reaction ^{9}Be(p,pn)^{8}Be has been studied at $E_o=45$ MeV [1], 46 MeV [2] and 1 GeV [3]. At $E_o=45$ MeV [1] the distortions are so strong that the $1s$ shell does not manifest itself in the separation energy spectra. At $E_o=1$ GeV distortions are weak and so this energy region is convenient to study the single-particle aspects of the nuclear structure. The reaction ^{9}Be($p,2p$)^{8}Li has been studied only for $E_o \geqslant 185$ MeV.

The energy region between 50 and 150 MeV is particularly interesting for the study of distortion effects in light nuclei, since in this case all shells already manifest themselves and the distortions are still strong. Experimental information about distortion effects can be obtained from the comparative analysis of simultaneous measurements, under identical kinematic conditions, of (p,pn) and ($p,2p$) reactions, since in this case some systematic experimental uncertainties are cancelled.

This work is a continuation of our study [4,5] of distortion effects in quasielastic knockout of nucleons by 70 MeV protons, and presents results of the simultaneous measurements of the cross sections for the reactions ^{9}Be(p,pn)^{8}Be and ^{9}Be($p,2p$)^{8}Li. An analysis of the cross sections for $1s$ and $1p$ shells in the framework of DWTA approach is also presented and the root-mean-square radius of ^{8}Be is derived.

II. EXPERIMENTAL PROCEDURE

The experiment was carried out using the 70 MeV proton beam from the U-240 isochronous cyclotron of the Institute for Nuclear Research of the Ukrainian Academy of Sciences. The experimental facility was described elsewhere [4–6].

A magnetic spectrometer was used for the momentum analysis of the scattered protons, at a fixed angle ($\theta_1 = 45°$) with respect to the initial beam axis. Momentum analyzed protons were detected in the focal plane by an 8-channel scintillation counter with momentum acceptance of $\pm 3\%$.

Protons and neutrons were detected in coplanar geometry by two spectrometers, located on opposite sides of the initial proton beam trajectory. Energies of the secondary particles (E_2, for protons and neutrons) were determined, at definite angles θ_2, by the time-of-flight spectrometer (TFS). The TFS consisted of five scintillation-counter telescopes, positioned uniformly along a circular arc covering the range $45° - 69°$, in steps of $\Delta\theta_2 = 6°$. Each telescope consisted of two plastic scintillators (NE102A), 5- and 200-mm thick, respectively, coupled with photomultipliers PM-36. Between the scintillators was placed a lead absorber 8-mm thick to avoid charged particles arriving at the second scintillator. The first scintillator detects practically only protons, since its neutron detection efficiency is very small ($\approx 0.3\%$). The second scintillator detects only neutrons (with about 10% efficiency, see Ref. [5]), since the protons were stopped at the absorber. Signals from the scintillators were used for timing purposes. The energies of the secondary particles were determined from the difference in flight time between them and the scattered protons detected by the magnetic spectrometer.

Three solid and self-supporting targets were used in the experiment: (i) polyethylene (CH_2), $2.13(2)\times10^{21}$ cm^{-2}, (ii) deuterium polyethylene (CD_2), $1.44(7)\times10^{21}$ cm^{-2}, and (iii) beryllium, (^{9}Be), $2.5(1)\times10^{21}$ cm^{-2}.

The CD_2 and ^{9}Be targets were prepared by pressing the

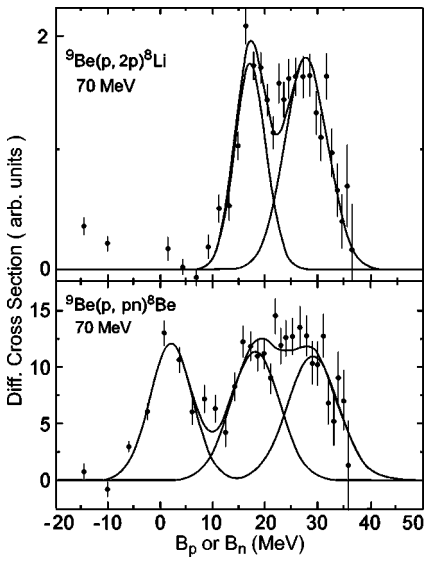

FIG. 1. Typical decomposition of $(p,2p)$ (upper part) and (p,pn) spectra, for one momentum bite of the spectrometer.

corresponding powders on an evacuated mold.

The CH_2 target was used in the calibration of the magnetic spectrometer. Energy scale and efficiency were both determined using the proton elastic cross sections on ^{1}H. The CD_2 target was used to calibrate several parameters. In particular, neutrons from the breakup of the deuteron were used to determine the efficiency of the neutron detectors.

The TDC spectra of pn- and pp-coincidences (time differences between signals from the magnetic and TFS spectrometers) were recorded by the acquisition system in event-by-event mode.

The pn- and pp-coincidence spectra as a function of the separation energies of the neutron (B_n) and proton (B_p), respectively, were decomposed in partial contributions from quasi-free knockout of $1s$ and $1p$ shells. The decomposition was based on a least-squares fit of two (pp-spectra) or three (pn-spectra) Gaussians to the experimental spectra, leaving two free parameters for each peak: height and FWHM. Peak positions were fixed according to the separation energies obtained in Ref. [3] at $E_0=1$ GeV: $B_p(1p)=17.1$ MeV and $B_p(1s)=27.7$ MeV for pp-spectra; and $B_n(1p)=1.98$ and 18.1 MeV and $B_n(1s)=29.2$ MeV for pn-spectra. Figure 1 shows, in the same scale, a typical decomposition of pn- and pp-coincidence spectra, with three and two peaks, respectively, for one momentum bite of the spectrometer.

III. THEORETICAL MODEL

The cross section for the ^{7}Li$(p,pn)^6$Li reaction was calculated in the distorted-wave approximation for non-local realistic t-matrix (DWTA). This method was first developed in the works of Refs. [7,8] and then improved [4,9,10] for the case of arbitrary geometry, eliminating ambiguities in the parameters and including indirect processes.

For the description of the nucleon-nucleon interaction it was used a second-rank non-local separable potential with Gaussian form factor. The parameters of the potential were determined making use of (p,p) and (p,n) phase-shift analysis data [11]. The potential gives a good description of the energy behavior of all phase shifts for s, p, d and f waves in the isotopic spin $T=0,1$ channels, and the corresponding mixing parameters in the energy range from 0 to 500 MeV. These parameters have been used to generate the t-matrix to calculate the cross section.

The distorted wave functions (DWF) for the entrance $(+)$ and exit $(-)$ channels, used in the calculation, incorporate refraction, absorption and focusing, and have an analytical representation similar to the eikonal approximation [4]:

$$\Psi^{+}_{\vec{k}}(\vec{r})=e^{-\gamma\vec{k}R_N}e^{i(\beta+i\gamma)\vec{k}\vec{r}}[1+Fe^{-(\vec{r}-R\hat{k})^2/S^2}]$$

and

$$\Psi^{-}_{\vec{k}}(\vec{r})=[\Psi^{+}_{-\vec{k}}(\vec{r})]^*,$$

where $\beta+i\gamma=D$ is the complex refractive index of the optical model. The quantity βk plays the role of a modified wave number, and γ determines the damping. F, R and S are focusing parameters. For the case of ^{9}Be, R_N can be chosen as the mass radius of the nucleus.

The DWF parameters can be unambiguously chosen [6] from the requirement of a quantitatively correct description of the experimental data for the total and elastic cross sections, for the interaction of a proton (neutron) with the corresponding nucleus in the entrance and exit channels, and additionally by requiring the agreement between the model DWF and the exact wave function, obtained by numerical integration of the Schrödinger equation in a range comparable with the size of the nucleus.

IV. RESULTS AND DISCUSSION

The differential (p,pn) and $(p,2p)$ cross sections for the $1p$ shells, as a function of θ_2, obtained from the decomposition procedure, are shown in Fig. 2, respectively by the full and light circles. Figure 3 shows the same for the $1s$ shell. The error bars of the experimental data shown in Figs. 2 and 3 represent both statistical and absolute uncertainties, since our aim is to make an absolute comparison with the theoretical calculations (for more details, see Ref. [5]).

From the data of Figs. 2 and 3, one can determine the ratio [3]:

$$\mathfrak{R}^A=\frac{d^3\sigma(p,pn)d\sigma(p,p)N_p^l}{d^3\sigma(p,2p)d\sigma(p,n)N_n^l},$$

where N_p^l and N_n^l are respectively the number of protons and neutrons in shell l, and $d\sigma(p,n)$ and $d\sigma(p,p)$ are the elastic scattering cross sections for these energies and angles. We used the same proton and neutron effective occupation numbers for the $1s$ and $1p$ shells (17−18 MeV) of ^{9}Be

$$\frac{N_p^{1s}}{N_n^{1s}}=\frac{N_p^{1p}}{N_n^{1p}}=1.$$

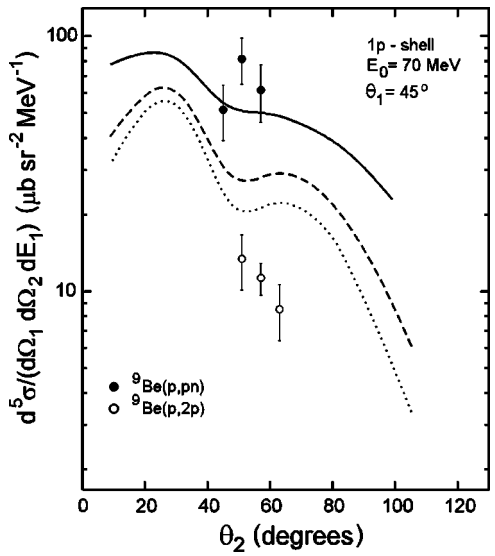

FIG. 2. The differential cross sections for the reactions ^{9}Be(p,pn)^{8}Be (full circles) and ^{9}Be($p,2p$)^{8}Li (light circles), at $E_0=70$ MeV and $\langle E_1\rangle=29$ MeV, for the $1p$ shells ($B_p=17.1$ MeV, $B_n=18.1$ MeV) versus θ_2. Distortion effects were corrected according to the emitted particle energy (see text and Ref. [5] for details). The dotted and dashed lines correspond to the contributions of direct mechanism and the coherent sum of direct and indirect mechanisms, respectively. The solid line represents results of the modified DWTA calculations (see text for details).

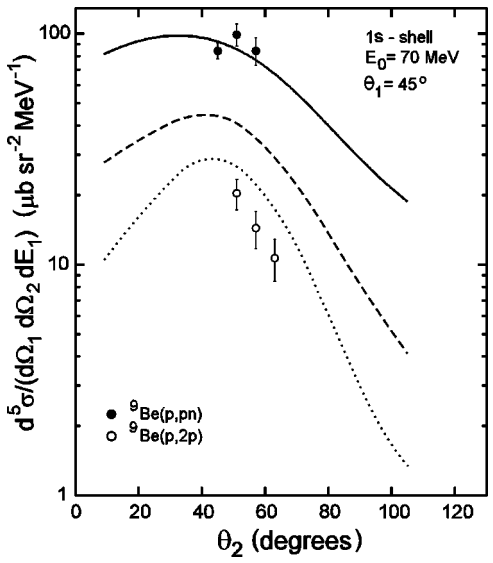

FIG. 3. The same as Fig. 2, but for the $1s$ shells.

This was based on the results obtained analyzing data [3] where the conditions of small off-shell and FSI distortions hold. At sufficiently high E_0, when the impulse approximation is valid, $\Re^A$ is defined by the single-particle bound state wave functions for protons and neutrons and, in the cases where proton and neutron distributions are identical, $\Re^A=1$. Deviations of $\Re^A$ from unity at high energies are connected with differences between the root-mean-square radii of the nuclear shells for protons ($r^p_{\rm rms}$) and neutrons ($r^n_{\rm rms}$) [12,13]. This dependence is strong since $\Re^A \propto (r^n_{\rm rms})^4/(r^p_{\rm rms})^4$ [3], and small differences in $r_{\rm rms}$ can result in large deviations of $\Re^A$ from unity. For $E_0 < 100$ MeV $\Re^A$ presents a strong deviation from the single-particle value as a result of distortion effects [14]. Table I shows the values of $\Re^A$ obtained from the world data for light nuclei for $E_0 \leqslant 100$ MeV, and $\theta_1=\theta_2=45°$, and also for $E_0=1$ GeV, where the values are associated with the single-particle mechanism. For ^{9}Be at $E_0=70$ MeV, $\Re^A$ presents a large deviation from the single-particle mechanism value. This deviation is connected with off-shell and FSI distortions.

Figure 4 shows the ^{9}Be(p,pn) cross sections, as a function of the momentum of the residual nucleus, k_{A-1}, for the $1p$ subshell ($B_n=1.98$ MeV, there is not an analogous subshell for protons). The open circles represent data taken at

TABLE I. Experimental values of $\Re^A$ (see text) for several nuclei and energies.

		Values of $\Re^A$					
E_o (MeV)		23	50	70	85	100	1000
Nucleus	Shell						
^{2}H	$1s$	2.5(2)[b]	1.4(1)[b]	1.1(1)[c]	0.9(1)[c]	0.9(1)[c]	1.01(3)[d]
^{3}He	$1s$		1.4(1)[c]			$\sim$1.0[d]	
^{4}He	$1s$			2.4(2)[f]			$\sim$1.0[d]
^{6}Li	$1p$		2.7(1)[g]	3.5(4)[h]			0.95(8)[d]
	$1s$			3.6(4)[h]			1.03(10)[d]
^{7}Li	$1p$			2.3(4)[i]			1.05(4)[d]
	$1s$			2.3(4)[i]			1.08(15)[d]
^{9}Be	$1p$[a]			3.9(15)[j]			1.58(5)[d]
	$1s$			3.9(12)[j]			0.97(12)[d]

[a] $B_n=18.1$ MeV.
[b] Reference [16].
[c] Reference [17].
[d] References [3,19].
[e] Reference [18].
[f] Reference [4].
[g] Reference [15].
[h] References [20,21].
[i] Reference [5].
[j] This work.

$E_0 = 70$ MeV (this work). Full circles represent data of Ref. [1] taken at 45 MeV, multiplied by 0.6 [ratio of free (p,n) cross sections at 70 and 45 MeV] and rearranged as a function of k_{A-1}. In spite of the differences between off-shell and FSI distortions at these energies, the data sets agree well both in magnitude and dependence on k_{A-1}. The agreement between the two sets of data might be explained by the inverse tendency in the behavior of FSI and off-shell effects versus E_0, resulting in a compensation of each other, as in the case of ^{7}Li [5,20].

For the reaction ^{9}Be$(p,pn)^8$Be it is impossible to carry out the DWTA calculation on the same realistic base as in the case of ^{7}Li$(p,pn)^6$Li [5] and ^{4}He$(p,pn)^3$He [4], since there are no data for the elastic and total cross sections of the reactions $(p,^8\mathrm{Be})$ and $(n,^8\mathrm{Be})$. But, as a first approximation, we can calculate the (p,pn) differential cross section by evaluating the FSI contribution using the cross section for ^{9}Be [21] instead of ^{8}Be in the calculation. The parameters of the distorted wave function for this case were obtained for $E_0 = 70$ MeV and three different scattered proton energies $\langle E_1 \rangle = 27$, 29, and 31 MeV, corresponding to the following average energies of the emitted particles:

$$\langle E_2 \rangle = \begin{cases} 41, 39, \text{ and } 37 \text{ MeV neutrons from } 1p \text{ shell } (N_n = 1.98 \text{ MeV}) \\ 25, 23, \text{ and } 21 \text{ MeV (protons or neutrons) from } 1p \text{ shell } (B_n \approx B_p \approx 18 \text{ MeV}) \\ 14, 12, \text{ and } 10 \text{ MeV (protons or neutrons) from } 1s \text{ shell } (B_n \approx B_p \approx 28 \text{ MeV}). \end{cases}$$

It should be stressed that the obtained set of DWF parameters is unambiguous, since it was chosen requiring the correct description of the elastic and total cross sections for the interaction of a proton (neutron) with the corresponding nucleus and also the agreement between our model DWF and the exact wave function, obtained by numerical integration of the Schrödinger equation over a range comparable to the size of the nucleus. The procedure used for the choice of parameters (and an analysis of their ambiguity) as well as the calculations of the cross sections are described in detail in Ref. [9]. Figures 2–4 show the results of such DWTA calculation of (p,pn) cross sections for $1s$ and both $1p$ subshells, carried out with DWF for ^{9}Be in the final state and the single-particle bound state wave functions for protons and neutrons, obtained for Woods-Saxon potential with parameters chosen from the correct description of the binding energies and form factors of ^{9}Be. The dotted curves show the contribution of the direct mechanism, and the dashed curves the coherent sum of direct and indirect mechanisms. In Fig. 4 only the coherent sum of direct and indirect mechanisms is shown, since the contribution of the indirect mechanism alone is very small at this kinematics.

It is clear from Figs. 2 and 3 that the DWTA calculations strongly underestimate the experimental data: a factor of 2.2 for the $1s$ shell, and of 2.3 for the $1p$ shell ($B_n = 18.1$ MeV). Only the results for the $1p$ shell ($B_n = 1.98$ MeV), shown in Fig. 4, present a better agreement, with the calculation being 10% lower than the data. This difference is associated with the difference between the final state interactions in ^{8}Be and ^{9}Be, since this is the only change in the standard DWTA calculation, which otherwise describes correctly the experimental cross sections without free parameters [4,5]. On the other hand, we know [7,22] that the DWF parameter, R, is directly proportional to the root-mean-square mass radius of the nucleus in the final state, and we improved the DWTA calculation by changing R, obtained for ^{9}Be, to $R' = R(r_{\mathrm{rms}}^{^8\mathrm{Be}}/r_{\mathrm{rms}}^{^9\mathrm{Be}})$, where $r_{\mathrm{rms}}^{^9\mathrm{Be}} = 2.96(8)$ fm is the root-mean-square mass radius of ^{9}Be [3] and $r_{\mathrm{rms}}^{^8\mathrm{Be}}$ is a parameter to be fitted. We obtained for $r_{\mathrm{rms}}^{^8\mathrm{Be}} = 2.52(7)$ fm. This value is very close to the root-mean-square radius of the charge distribution (core radius) of ^{9}Be (2.519 ± 0.012 fm [23]) and can be associated with the mass radius of ^{8}Be.

This result is similar to that obtained for ^{12}C and ^{13}C, where the root-mean-square value of the mass radius $r_{\mathrm{rms}}^n = 2.41(2)$ fm [24], for ^{12}C, is very close to the value of the charge radius $r_{\mathrm{rms}}^p = 2.440(25)$ fm [25], for ^{13}C; and also to the case of ^{16}O and ^{17}O, where the mass radius $r_{\mathrm{rms}}^n = 2.65(4)$ fm, for ^{16}O [26], and the charge radius $r_{\mathrm{rms}}^p = 2.662(26)$ fm [27], for ^{17}O, are very close. Final results of these DWTA calculations are shown in Figs. 2–4 by the solid lines. This new calculation gives a quantitatively adequate description of the differential cross sections for $1s$

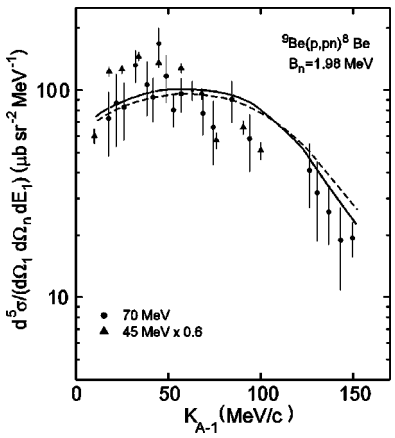

FIG. 4. The differential cross section for the reaction ^{9}Be$(p,pn)^8$Be, for the $1p$ shell ($B_n = 1.98$ MeV). Full circles represent data of the present work at $E_0 = 70$ MeV, and $\langle E_1 \rangle = 29$ MeV; triangles are from Ref. [1], for $E_0 = 45$ MeV. Dashed and solid lines represent results of DWTA calculation as in Fig. 2, but for $B_n = 1.98$ MeV (see text for details).

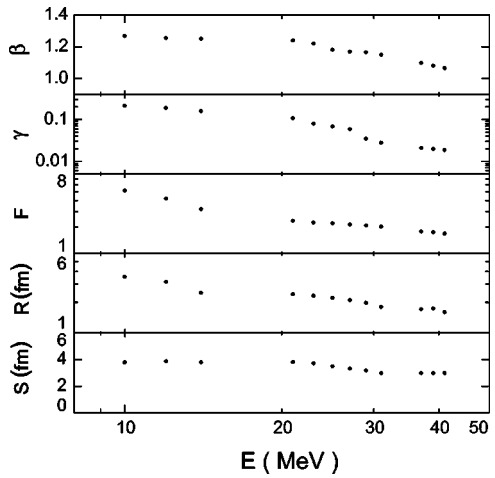

FIG. 5. The DWF parameters for ^{8}Be as a function of the outgoing particle (proton or neutron) energy.

and both $1p$ subshells, which have different relative contributions from FSI and off-shell effects. One should also note that the change in the radius increases the differential cross sections of different subshells by different amounts, achieving good agreement with the experimental data. This indicates that the new set of DWF parameters is realistic.

Between 10 and 41 MeV, the DWF parameters for ^{8}Be in the final state present dependences with the energy of the outgoing particle, E_2, that can be well represented by smooth functions (see Fig. 5). Note that the DWF parameters are the same for protons or neutrons, since the Coulomb contribution is negligible.

The obtained set of DWF parameters can be used for the reconstruction of the optical potential for ^{8}Be, following the calculation scheme of Ref. [10].

For the reaction ^{9}Be$(p,2p)^8$Li it is impossible to carry out the standard DWTA calculation, since there are no data for the elastic and total cross sections of the reactions $(p,^8\mathrm{Li})$ and $(n,^8\mathrm{Li})$. Furthermore, we cannot fulfill an analysis similar to that performed for the reaction ^{9}Be$(p,pn)^8$Be, since the available data for the cross section of the reaction $(p,^7\mathrm{Li})$ are not sufficient for an unambiguous choice of a set of DWF parameters.

Nevertheless some interesting conclusions can be drawn from the analysis of the ratio of (p,pn) to $(p,2p)$ cross sections of ^{9}Be (see Table II), which were measured simultaneously and under identical kinematical conditions. This experimental ratio contains information about differences in FSI effects connected with different exit channels, and differences in off-shell effects associated with differences in the p and n separation energies. Adding to that results of the DWTA calculations [4,5] (obtained with the appropriate cross section input data), which reproduce correctly the experimental (p,pn) and $(p,2p)$ cross sections without any free parameters, we can estimate the order of magnitude of the FSI and off-shell effects in this ratio. In particular, it is possible to evaluate the sensitivity of the FSI correction to the characteristics of the final nucleus. To do this, we calculate the ^{9}Be$(p,2p)^8$Li cross section with a hypothetical final state interaction, using for the DWF in the exit channel the set of parameters obtained for ^{8}Be, instead of ^{8}Li, keeping unchanged all another DWTA parameters (off-shell nucleon-nucleon interaction t matrix, and DWF for the entrance channel). Table II presents the experimental ratio, $\mathfrak{R}^A$ for several nuclei, obtained at $E_0=70$ MeV, and the ratio

$$\mathfrak{R}^{\mathrm{FSI}}=\frac{d^3\sigma(p,2p)^{\mathrm{hyp}}}{d^3\sigma(p,2p)^{\mathrm{expt}}},$$

for different energy combinations of the nucleons in the exit channel. This ratio characterizes the importance of the distortions caused by FSI effects. If these effects were negligible (or identical for both ^{8}Be and ^{8}Li) this ratio should be equal to 1. Table II shows the high sensitivity of the cross section ratio to FSI effects. The change of ^{8}Li to ^{8}Be (Coulomb effects are negligible in our kinematical conditions [5]) increases the cross section ratio to 3.5. Table II also shows the ratio

TABLE II. Values of $\mathfrak{R}^{\mathrm{off\text{-}shell}}$, $\mathfrak{R}^{\mathrm{FSI}}$, and $\mathfrak{R}^A$ (see text) for several nuclei at 70 MeV.

Nucleus	Shell	B (MeV)	$\langle E_1\rangle;\langle E_2\rangle$ (MeV)	$\mathfrak{R}^{\mathrm{off\text{-}shell}}$ $\frac{(p,pn)^{\mathrm{expt}}(pp)_{el}}{(p,2p)^{\mathrm{hyp}}(pn)_{el}}$	$\mathfrak{R}^{FSI}$ $\frac{(p,2p)^{\mathrm{hyp}}}{(p,2p)^{\mathrm{expt}}}$	$\mathfrak{R}^A$ $\frac{(p,pn)(pp)_{el}}{(p,2p)(pn)_{el}}$	$\mathfrak{R}^A$ @1000 MeV
^{9}Be	$1p$	2	23; 29	1.1[d]			
^{7}Li	$1p$	9	30; 30	1.2[c]			1.05(4)[a]
^{7}Li	$1p$	9	22; 40	1.1[c]	1.7(3)[c]	2.3(4)[c]	1.05(4)[a]
^{9}Be	$1p$	18	29; 39	0.85[d]	3.0(8)[d]	3.9(15)[d]	1.58(5)[a]
^{4}He	$1s$	21	25; 25	0.6[b]	3.6(2)[b]	2.1(2)[b]	$\sim$1.0[b]
^{7}Li	$1s$	25	22; 22	0.6[c]	3.9(4)[c]	2.3(4)[c]	1.08(15)[a]
^{7}Li	$1s$	25	30; 14	0.7[c]	2.2(4)[c]	2.0(4)[c]	1.08(15)[a]
^{9}Be	$1s$	28	29; 12	0.6[d]	6.0(14)[d]	3.9(2)[d]	0.97(12)[a]

[a]Reference [3].
[b]References [4,5].
[c]Reference [5].
[d]This work.

$$\Re^{\text{off-shell}} = \frac{d^3\sigma(p,pn)^{\text{expt}} d\sigma(p,p)_{el}}{d^3\sigma(p,2p)^{\text{hyp}} d\sigma(p,n)_{el}},$$

which characterizes the relative contribution of the off-shell effects in the cross sections, since in $d^3\sigma(p,2p)^{\text{hyp}}$ we have the same entrance and exit channels as in $d^3\sigma(p,pn)^{\text{expt}}$, the only change being connected with the difference in off-shell effects due to the difference in the p and n separation energies. If the off-shell effects were negligible (or identical) this ratio should be equal to 1. In Table II the ratios are arranged in order of increasing separation energies, B. One can see that $\Re^{\text{off-shell}}$ decreases with the increase of B, while $\Re^{\text{FSI}}$ presents the opposite tendency, as expected.

V. CONCLUSIONS

The process of quasifree knockout of nucleons from ^{9}Be already manifests the contribution of all shells at $E_0 = 70$ MeV, and it is possible at this energy to separate and to study, independently, these contributions.

The ratio of the differential cross sections of the reactions ^{9}Be$(p,pn)^8$Be and ^{9}Be$(p,2p)^8$Li for $1s$ and $1p$ shells at $E_0 = 70$ MeV is significantly larger than for other light nuclei studied. This ratio is the same for $1s$ and $1p$ shells and shows that, within the experimental conditions, the dependence of FSI and off-shell effects with separation energy have opposite tendencies and, as a result, the ratio is practically the same for $1s(B_n = 29.2$ MeV, $B_p = 27.7$ MeV) and $1p(B_n = 18.1$ MeV, $B_p = 17.1$ MeV) shells.

The DWTA calculations give a quantitatively correct description of the differential cross sections for the reaction ^{9}Be$(p,pn)^8$Be at $E_0 = 70$ MeV for $1s$ and both $1p$ subshells, if the radius of ^{8}Be is supposed to be equal to the core radius of ^{9}Be. This means that the models used for FSI and off-shell effects are realistic for light nuclei in the energy range under study.

As FSI is very sensitive to the specific characteristics of the final state system, even for a constant atomic number, exotic few-nucleon systems can be studied through this kind of experiment.

[1] C.N. Waddell *et al.*, Nucl. Phys. **A281**, 418 (1977).
[2] C.A. Miller, J.W. Watson, D.I. Bonbright, F.J.S. Wilson, and D.O. Wells, Phys. Rev. Lett. **32**, 684 (1974).
[3] C.L. Belostotskii *et al.*, Yad. Fiz. **41**, 1425 (1985) [Sov. J. Nucl. Phys. **41**, 903 (1985)]; C.L. Belostotskii *et al.*, Leningrad Institute of Nuclear Physics Report No. 867 (1983).
[4] M.V. Pasechnik *et al.*, Yad. Fiz. **54**, 616 (1991) [Sov. J. Nucl. Phys. **54**, 373 (1991)].
[5] V.B. Shostak, G.P. Palkin, N.I. Woloshin, V.P. Likhachev, J.D.T. Arruda-Neto, M.T.F. da Cruz, and M.N. Martins, Nucl. Phys. **A643**, 3 (1998).
[6] V.B. Shostak, V.P. Badjvskij, G.P. Palkin, C.M. Khoromanskij, and V.P. Likhachev, Appl. Nucl. Spectrosc. **13**, 106 (1984) (collection of articles, Anargoatomizdat, Leningrad, 1984).
[7] P.C. Wright, R.G. Storer, and I.E. McCarthy, Phys. Rev. C **17**, 473 (1978).
[8] R.T. Janus and I.E. McCarthy, Phys. Rev. C **10**, 1041 (1974).
[9] M.I. Voloshin and A.D. Fursa, Ukr. Phys. J. **39**, 1036 (1994).
[10] M.I. Voloshin and A.D. Fursa, Ukr. Phys. J. **40**, 1171 (1995).
[11] R.G. Arndt, L.D. Roper, R.A. Bryan, R.B. Clark, B.J. VerWest, and P. Signell, Phys. Rev. D **28**, 97 (1983).
[12] H.B. Hkansson, T. Berggren, and R. Bengtsson, Nucl. Phys. **A306**, 406 (1978).
[13] A.N. James, W.J. McDonald, J.M. Cameron, C.A. Miller, D.A. Hutcheon, P. Kitching, G.C. Neilson, G.M. Stinson, and E.D. Earle, Nucl. Phys. **A324**, 253 (1979).
[14] C.A. Miller, D.I. Bonbright, J.W. Watson, and F.J. Wilson, in *Few Particle Problems in the Nuclear Interaction*, edited by I. Slaus, S.A. Moszkowski, R.P. Haddock, and W.T.H. van Oers (North-Holland, Amsterdam, 1972), p. 189.
[15] J.L. Durand, J. Arvieux, A. Fiore, C. Perrin, and M. Durand, Phys. Rev. C **6**, 393 (1972).
[16] V.K.C. Cheng and P.G. Roos, Nucl. Phys. **A225**, 397 (1974).
[17] M.V. Pasechnic *et al.*, Ukr. Phys. J. **36**, 659 (1991).
[18] M.V. Pasechnic *et al.*, Ukr. Phys. J. **33**, 976 (1988).
[19] A.I. Vdovin *et al.*, Izv. Akad. Nauk CCCP, Ser. Fiz. **47**, 2219 (1983).
[20] M.I. Voloshin *et al.*, Izv. Akad. Nauk CCCP, Ser. Fiz. **57**, 218 (1993).
[21] J.W. Verba, H. Willmes, R.F. Carlson, I. Slaus, J.R. Richardson, and E.L. Petersen, Phys. Rev. **153**, 1127 (1967); T.Y. Li and S.K. Mark, Can. J. Phys. **46**, 2645 (1968); G.S. Mani, D. Jacques, and A.D.B. Dix, Nucl. Phys. **A165**, 145 (1971); D.G. Montague, R.K. Cole, P.S. Lewis, C.N. Waddell, and D.L. Hendrie, *ibid.* **A199**, 433 (1973); L. Sihver, C.H. Tsao, R. Silberberg, T. Kanai, and A.F. Barghouty, Phys. Rev. C **47**, 1225 (1993); H.J. Votava, T.B. Clegg, E.J. Ludwig, and W.J. Thompson, Nucl. Phys. **A204**, 529 (1973).
[22] A.I. Vdovin, A.B. Golovin, I.I. Loshchakov, Yad. Fiz. **42**, 134 (1985) [Sov. J. Nucl. Phys. **42**, 84 (1985)].
[23] J.A. Jansen, R.Th. Peerdeman, and C. de Vries, Nucl. Phys. **A188**, 337 (1972).
[24] I. Sick and J.S. McCarthy, Nucl. Phys. **A150**, 631 (1970).
[25] J. Heisenberg, J.S. McCarthy, and I. Sick, Nucl. Phys. **A157**, 435 (1970).
[26] D. Vautherin and D.M. Brink, Phys. Rev. C **5**, 626 (1972).
[27] R.P. Singhal, J.R. Moreira, and H.S. Caplan, Phys. Rev. Lett. **24**, 73 (1970).